



Citation for published version:

Pan, L, Liu, Z, Tian, M, Schroeder, B, Aliev, AE & Faul, CFJ 2019, 'Luminescent and Swellable Conjugated Microporous Polymers for Detecting Nitroaromatic Explosives and Removing Harmful Organic Vapors', *ACS Applied Materials and Interfaces*, vol. 11, no. 51, pp. 48352-48362. <https://doi.org/10.1021/acsami.9b16767>

DOI:

[10.1021/acsami.9b16767](https://doi.org/10.1021/acsami.9b16767)

Publication date:

2019

Document Version

Peer reviewed version

[Link to publication](#)

This document is the Accepted Manuscript version of a Published Work that appeared in final form in *ACS Appl. Mater. Interfaces*, copyright © American Chemical Society after peer review and technical editing by the publisher. To access the final edited and published work see <https://pubs.acs.org/doi/10.1021/acsami.9b16767>.

University of Bath

Alternative formats

If you require this document in an alternative format, please contact:
openaccess@bath.ac.uk

General rights

Copyright and moral rights for the publications made accessible in the public portal are retained by the authors and/or other copyright owners and it is a condition of accessing publications that users recognise and abide by the legal requirements associated with these rights.

Take down policy

If you believe that this document breaches copyright please contact us providing details, and we will remove access to the work immediately and investigate your claim.

**Luminescent and Swellable Conjugated Microporous
Polymers for Detecting Nitroaromatic Explosives and
Removing Harmful Organic Vapors[†]**

Long Pan,^a Zilu Liu,^b Mi Tian,^c Bob C. Schroeder,^b Abil E. Aliev,^b

Charl F. J. Faul^{a,*}

^a *School of Chemistry, University of Bristol, Bristol, England BS8 1TS, U.K.*

^b *Department of Chemistry, University College London, London WC1H 0AJ,
U.K.*

^c *Department of Chemical Engineering, University of Bath, Claverton Down,
Bath, BA2 7AY, U.K.*

[†] Electronic Supplementary Information (ESI) available:

Keywords:

conjugated microporous polymers, detection of nitroaromatic, swellability, methanol adsorption, fluorescence

Abstract

Four new conjugated microporous polymers (CMPs) were synthesised by Buchwald-Hartwig cross-coupling reaction of tri- and tetra- functionalised precursors to yield materials with tuneable surface area and pore size distribution. This approach yielded **LPCMP1–4**, CMPs with significantly higher Brunauer–Emmett–Teller (BET) surface area (more than five times higher) than other related BH-based CMPs. These CMP materials possess not only high BET specific surface areas and high chemical and thermal stabilities, but also exhibit outstanding swellability. To the best of our knowledge, swellable behaviour was studied in great detail for CMPs for the first time, with the greatest degree of swelling for methanol reaching 16.5 and 16.3 mL g⁻¹ for **LPCMP1** and **LPCMP3**, respectively. Owing to their excellent swellability, we further studied the adsorption capacity of these CMPs for different toxic organic vapours (including toluene and methanol). **LPCMP1** and **LPCMP3** adsorbed 124 mg g⁻¹ and 117 mg g⁻¹ respectively, toluene at its saturated vapor pressure. For methanol, the adsorption capacities of **LPCMP1** and **LPCMP3** were up to 250 mg g⁻¹ and 215 mg g⁻¹, respectively, which is the highest recorded value when compared with published data for CMPs, HCPs, MOFs and porous carbons. These materials are promising candidates for the removal and elimination of hazardous organic vapors and chemical warfare agents. Moreover, all the polymers show high sensitivity to nitroaromatic explosives. **LPCMP2** **LPCMP4**, exhibit high selectivity for TNT, and may be suitable as new candidates to selectively detect TNT for security or environmental applications.

Introduction

Porous organic polymers (POPs) are a class of highly crosslinked porous polymers mainly composed of light elements such as C, N, O, H and B. These polymers show outstanding chemical and physical stability, high surface area, well-defined porosity and low skeletal density.¹ Owing to their exceptional properties, a large number of POPs have already been prepared, including conjugated microporous polymers (CMPs),^{2,3} covalent organic frameworks (COFs),^{4,5} polymers of intrinsic micro-porosity (PIMs),^{6,7} porous aromatic frameworks (PAFs)⁸ and hyper-crosslinked polymers (HCPs).⁹

Among these, CMPs permit the linking of building blocks in a π -conjugated fashion and possess three-dimensional (3D) networks. A range of different types reactions, including Suzuki,¹⁰ Sonogashira–Hagihara,¹¹ Yamamoto,¹² ethynyl trimerization reactions,¹³ Scholl,¹⁴ direct arylation,^{15,16} as well as various oxidative coupling polymerizations^{17,18,19} have been applied to synthesize CMPs. Buchwald–Hartwig (BH) coupling has also been utilized in CMP design and synthesis, where C–N bonds are created in the polymer network by the palladium-catalysed cross-coupling of (aryl)amines with aryl halides.^{20,21} This coupling approach also provides a simple route to develop N-rich redox-active CMPs. Compared with MOFs, the strong covalent bonds formed by these coupling reactions afford attractive properties, including higher thermal and chemical stabilities. Compared to non π -conjugated HCPs and COFs, the extended π -conjugated nature of the networks endows them with unique electron-donating characteristics and good luminescence properties.²² Unlike porous carbon materials, the vast choice of organic building blocks with different functional groups that have been used to synthesize CMPs not only allow fine-tuning of the specific surface area and porosity of the polymers, but also provide impressive diversity of properties and functionalities.²³ Recently, a new approach, named the Bristol-Xi'an Jiaotong (BXJ) approach, which can full synthetic control of the surface area and porosity of **PTPA** CMPs by the addition of salts, was reported

by our group.²⁴ Owing to these outstanding features, CMPs have shown great potential for application in gas adsorption and separation,²⁵ chemosensors,^{26,27} photocatalysis²³ and energy storage.²¹

Swellability, one of the lesser-known physical properties of crosslinked porous polymers, has not been studied thoroughly, nor attracted significant attention. In contrast to MOFs and porous carbon materials, the high number of links introduced by the crosslinking reaction provides the opportunity to create weak inter-chain interactions during removal of the reaction solvent to form the dry polymer network.²⁸ The internal stress created during the drying process can be relieved by the polymeric network allowing for the expansion of the formed structure, thus creating a swellable porous network. The swellability can be affected by several parameters, including the initial monomer concentration,²⁹ the extent of crosslinking and the solvation state of the growing polymer chains (nature of reaction solvent) during the polymerisation.³⁰ The polarity of the polymer will also influence its swellability.³¹ The swellability of HCPs has led to their use in various applications such as trapping of organic vapors,³² ion exchange,³³ removal of toxic trace metals,³⁴ solid phase extraction,³⁵ and recovery of organic pollutants from water.³⁶

Keeping applications in mind, detection of nitroaromatic explosives has become a critical issue and attracted substantial interest for public security, environmental safety and military applications.³⁷ Detecting explosives in solution, in addition to detection in the vapour phase, is also critical.³⁸ Trinitrotoluene (TNT), as one of the most commonly and widely used explosives for military, industrial, and mining applications, is considered a serious environmental contaminant with potential harmful and toxic effects on animals, plants, and humans.^{39,40} Thus, it is crucial to detect TNT and its derivatives as early as possible in soil, groundwater, or waste streams. Fluorescent CMPs have attracted attention for use in chemical sensors owing to their

high specific surface area, permanent porosity, good chemical and physical stability.⁴¹ However, there are limited reports about luminescent CMPs used for the detection of nitroaromatic compounds,^{26,27} and therefore provides further opportunities for the introduction of new materials for this important application area. As building blocks show great influence on the fluorescent properties, the design and selection of specific monomers is crucially important for the synthesis of fluorescent CMPs. Triphenylamine (TPA) has usually been selected as the main luminescent unit because of its low cost and electron-rich character. For example, two TPA-based fluorescent CMPs named PTPATTh and PTPATC were synthesised by using tris[4-(2-thienyl)phenyl]amine (TPATTh) and tris(4-carbazoyl-9-ylphenyl)amine (TPATCz) as monomers.⁴² Because of the aggregation-induced emission (AIE) properties of tetraphenylethylene (TPE)-based luminophores that can significantly increase the fluorescence quantum yields of the polymers and improve photoluminescence intensity, TPE is another important luminescent unit for fluorescent CMPs synthesis. Han et al. obtained TPE-based CMPs through palladium-catalyzed Suzuki coupling polymerization and oxidative coupling polymerization. Introducing the TPE units into the backbones afforded these polymers with strong fluorescence (λ_{max} : 530–610 nm) in the solid state.⁴³

Inspired by these developments and potential applications, and keen to continue to exploit the Buchwald–Hartwig (BH) cross-coupling strategy for CMP production, we here extend the amine-CMP family by using 1,3,5-tris(4-bromophenyl)amine (TBPA), tetrakis(4-bromidephenyl)ethylene (TBPE), 1,3,5-tris(4-aminophenyl)benzene (TAPB) and 1,3,5-tris-(4-aminophenyl)triazine (TAPT) as building blocks (please see **Figure S14** for other cores and linkers employed in our earlier investigations). The approach to date has been to select and combine cores with multiple Br groups and various di-amine linkers. In this study, we expand our synthetic approach and designed a range of new materials: we use combinations of tri- and tetrabromo and -amine building blocks (see Scheme 1), based on TPA and TPE, to synthesize

four novel BH CMPs and exploit the universal adaptability of our BXJ method for the control and optimization of the surface area, pore size and porosity. We then show how we utilise these materials and their novel properties for a wide range of applications.

Experimental Section

General Information: Synthesis of 1,3,5-tris-(4-aminophenyl)triazine (TAPT) and tetrakis(4-bromidephenyl)ethylene (TBPE) was shown in Supporting Information (S-3). Solid-state and liquid-state ultraviolet visible near-infrared (UV-vis/NIR) was recorded on a Shimadzu UV-2600 spectrometer. Fourier transform infrared (FT-IR) spectra were recorded on a PerkinElmer Spectrum 100 spectrometer. The ^1H and ^{13}C NMR spectra of all organic compounds were obtained on a Jeol Eclipse-400 (400 MHz). Solid-state ^{13}C NMR spectra were recorded on a Bruker Avance 300 spectrometer with 7.05 T wide-bore magnet at ambient probe temperature at 75.5 MHz, using a Bruker 4 mm double-resonance magic-angle spinning (MAS) probe and zirconia rotors spun at the MAS frequency of 12 kHz with stability better than ± 3 Hz. Cross-polarisation (CP) from protons was used for enhanced ^{13}C sensitivity. Typical acquisition conditions for ^{13}C CPMAS experiments were: ^1H 90° pulse duration = 2.68 μs ; contact time = 2 ms; recycle delay = 5 s. ^{13}C chemical shifts are given relative to tetramethylsilane, which was calibrated using glycine (176.46 ppm). Thermogravimetric analysis (TGA) was carried out on a TGA Q500 apparatus under a nitrogen atmosphere (flow rate 30 mL min^{-1}) by heating (10 $^\circ\text{C}$ min^{-1}) the samples to 800 $^\circ\text{C}$. Scanning electron microscopy (SEM) was performed using a JEOL JSM-IT300 Scanning Electron Microscope. X-ray photoelectron spectra (XPS) were obtained on a Thermo Scientific K-Alpha X-ray photoelectron spectrometer under ultrahigh vacuum ($< 5 \times 10^{-8}$ Torr) and by using a monochromatic Al $K\alpha$ X-ray source.

Porosities studies and adsorption measurements: All the samples were degassed at 120 $^\circ\text{C}$ for 12 h before measurement. Gas (nitrogen and carbon dioxide) sorption isotherms were recorded with a Quantachrome Autosorb iQ at set temperatures (at 77 K for N_2 , at 273 K for CO_2). Brunauer–Emmett–Teller (BET) specific surface area were calculated based on the obtained adsorption–desorption isotherms. The pore size distribution (PSD) profile of obtained materials was calculated from the related adsorption branch by the nonlocal density function

theory (NLDFT) approach. Total pore volume was calculated from nitrogen adsorption–desorption isotherms at $P/P_0 = 0.99$. The toluene and methanol vapor adsorption–desorption isotherms were performed and measured on an IGA-200 intelligent gravimetric analyzer (Hiden Isochema Ltd., UK) at room temperature (298K).

Synthesis of polymers LPCMP1–4: LPCMP1–4 were synthesized using a palladium-catalysed BH cross-coupling reaction. In order to establish the ideal polymerization conditions, different solvents, times and monomer ratios were tried as a series of optimization experiments. A typical procedure for the synthesis of LPCMP1 is provided here. A Schlenk tube was charged with tris(4-bromophenyl)amine (TBPA) (0.8 mmol, 433.8 mg, 1.5 equiv), 1,3,5-Tris(4-aminophenyl)benzene (TAPB) (0.6 mmol, 210.6 mg, 1 equiv), Pd(dba)₂ (dba = dibenzylideneacetone, 40.0 mg, 0.07 mmol, 8 mol %), 2-dicyclohexylphosphino-2',4',6'-triisopropylbiphenyl (XPhos) (50.1 mg, 0.045 mmol, 12 mol %), sodium tert-butoxide (NaOtBu) (461.3 mg, 4.8 mmol, 8 equiv) and sodium nitrate (0.8 mmol, 68 mg). The mixture was degassed and purged with nitrogen. Anhydrous tetrahydrofuran (THF) (50 mL) was added, and the reaction mixture was heated under stirring to 65 °C. After 48 h, the reaction was cooled to room temperature and 50 mL of methanol was added to the resulting mixture and stirred for 1 h. The obtained suspension was filtered, and the residue washed with methanol. The expected polymer was subsequently obtained after Soxhlet extraction in methanol, THF and chloroform (24 h each) and subsequent drying overnight in vacuo at 50 °C (yield: 98 %).

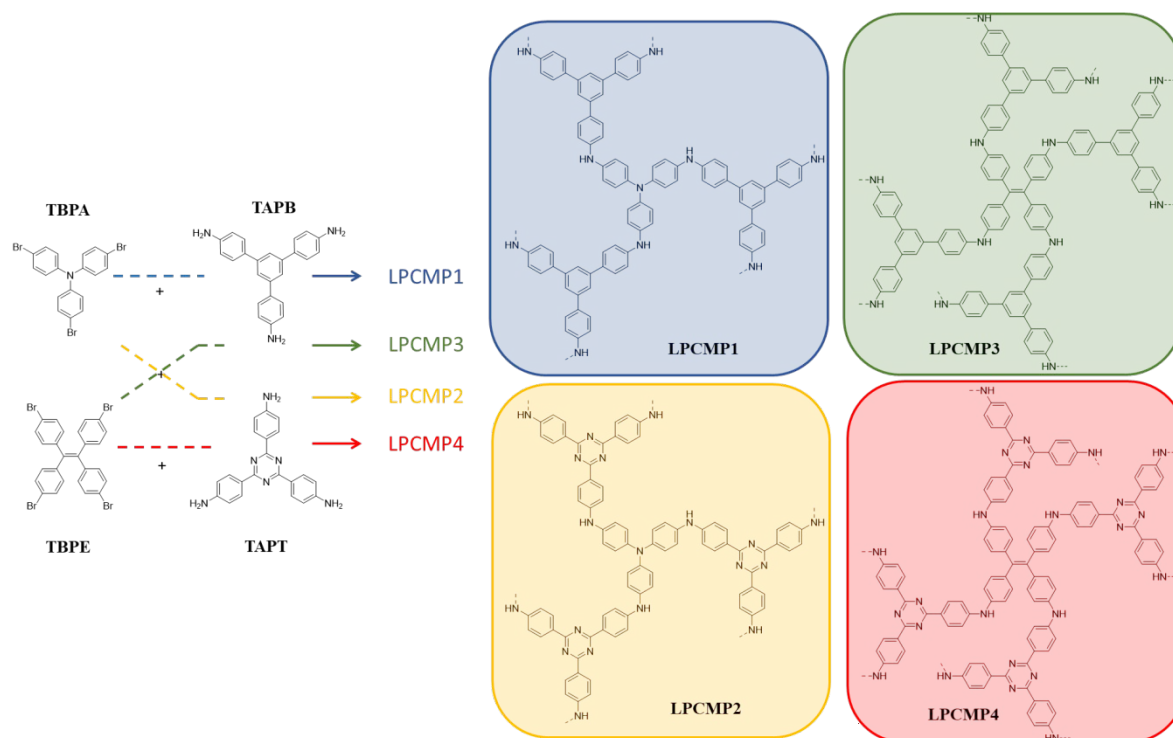
Synthesis of LPCMP2–4: After the optimization, the best reaction conditions are listed below: THF was used as solvent for the all synthesis procedure. The same inorganic salt (sodium nitrate) was added for the all synthesis procedure, and the molar ratio between the salt and bromine building block is 1:1. The same amount of Pd(dba)₂ (40.0 mg, 0.07 mmol, 8 mol %), XPhos (50.1 mg, 0.045 mmol, 12 mol %), NaOtBu (461.3 mg, 4.8 mmol, 8 equiv) were used for the all synthesis procedure. For LPCMP2, the TBPA (0.8 mmol) and TAPT (0.8 mmol)

was used. For **LPCMP3**, TBPE (0.6 mmol) and TAPB (0.6 mmol) was used. For the **LPCMP4** TBPE (0.6 mmol) and TAPT (0.8 mmol) was used.

Detection of explosives: To explore the sensing properties of the CMPs for nitroaromatic explosives, the fluorescence spectra of THF suspensions of **LPCMP1–4** (10 mg L^{-1}) were recorded after successive addition of TNT (standard solution from Aldrich), 4-nitrophenol (NP), 1,2-dinitrobenzene (DNB), 2,4-dinitrotoluene (DNT) and nitrobenzene (NB).

Swellability tests: In order to confirm the specific swellability, a swelling testing method reported by Adams et al was used.³⁶ Both polymers were ball milled into a fine powder prior to a swelling test (repeated three times). To a centrifuge tube (1.5 mL) a known mass of CMP was added (20 mg). The chosen solvent (1 mL) was added, the polymer allowed to stand in the solvent for 18 hours and the height of the swollen polymer in the tube measured. The obtained height measurements could be converted to the volume occupied by the polymer in the tube. The swellability (Q) of the polymer was defined by the final volume of the swollen polymer (mL) divided by the mass of polymer used (g).

Result and Discussion.

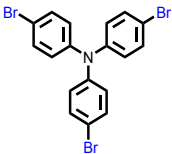

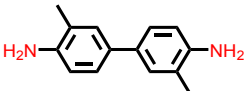
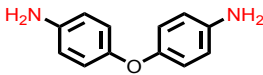
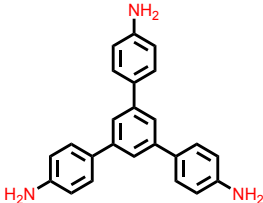


Scheme 1. Synthetic route of **LPCMP1-4**

The synthesis route for the four CMPs is depicted in **Scheme 1**. A series of optimization experiments were performed for the synthesis of **LPCMP1-NS** (no added inorganic salt) in order to obtain the highest yield and specific surface area. As shown in Table S1, different solvents, variation of the concentrations and ratio of the two building blocks were investigated and the best yield observed was 62% with a surface area of $275 \text{ m}^2 \text{ g}^{-1}$. A comparison of the **LPCMP1-NS** with other CMPs obtained by BH cross coupling of a brominated core and diamine linker pattern is shown in **Table 1**. The **LPCMP1-NS**, which was synthesized using the triamine building block, exhibited a significantly higher BET surface area (more than five times higher) than the other BH-based CMPs which were synthesized using the same core. Full synthetic control of the surface area and porosity of BH-based CMPs by the addition of inorganic salts, the so-called Bristol-Xi'an Jiaotong (BXJ) method, was reported by our group recently.²⁴ We found that the addition of simple salts tuned the Hansen solubility parameters

(HSPs) of the solvents to match that of the growing polymer chains, leading to CMPs with significantly higher surface areas and well-defined micropores. In order to further improve the surface area of **LPCMP1**, sodium nitrate (NaNO_3) was thus added to the reaction system. The yield increased from 62% to 98% and the BET specific surface area increased dramatically from $275 \text{ m}^2 \text{ g}^{-1}$ to $1280 \text{ m}^2 \text{ g}^{-1}$. Similar optimization experiments were also performed for the remaining CMPs and the final reaction conditions are shown in the experimental section.

Table 1. A comparison of the **LPCMP1-NS** with the other CMPs which were synthesized using the same core.

Core	Linker	S_{BET} ($\text{m}^2 \text{ g}^{-1}$)	Ref
		52	44
		62	44
		44	unpublished
		275	This work

The thermal stability of the polymers was studied (**Figure S3**); all the polymers possess good thermal stability and $\sim 5\%$ mass loss was observed from 300 to 370 °C under a nitrogen atmosphere. Owing to their cross-linked nature, there are no distinct transitions until 800 °C. SEM images of the polymers are presented in **Figure S4**, showing micrometer-sized amorphous polymer particles.

The suspension UV–Vis absorption spectra of **LPCMP1-4** are shown in **Figure 1** (a). Compared with **LPCMP1** and **LPCMP3**, a redshift of the absorption of **LPCMP2** and **LPCMP4** which were synthesized by using 1,3,5-tris-(4-aminophenyl)triazine instead of

1,3,5-Tris(4-aminophenyl)benzene was observed. The $-C=N-$ moiety is an ideal electron acceptor in triazine-based polymers⁴⁵ and this red shift might be explained by the doping effect of the acceptor co-monomer, as proved by Cooper et al.⁴⁶ The redshift led the calculated optical gap from 2.8 eV for **LPCMP1** to 2.3 eV for **LPCMP2** and 2.6 eV for **LPCMP3** to 2.4 eV for **LPCMP4**, and shows that it is possible to tune the optical gap by choosing the different building blocks. Similar trends were found for the photoluminescence emission spectra of **LPCMP1–4** as shown in **Figure 1** (b). As a result of the different optical band gaps, emission peaks at 500 nm, 558 nm, 536 nm and 611 nm, respectively, were observed. The photoluminescence was tuned from light green fluorescence to brown fluorescence.

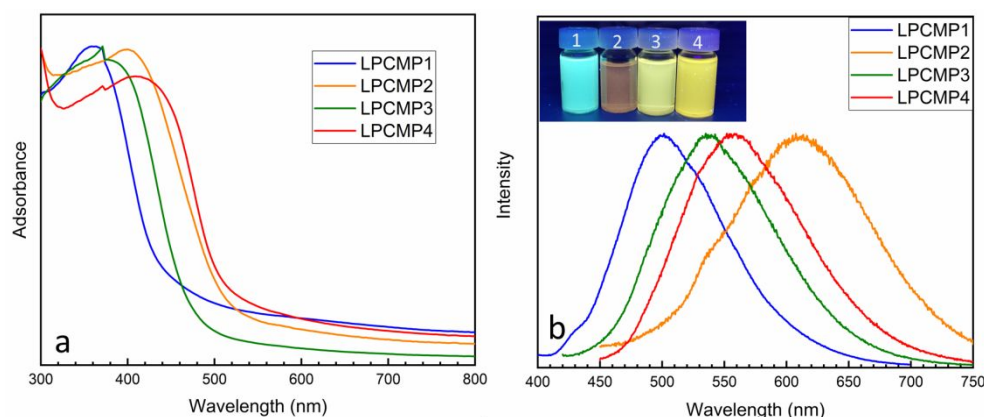


Figure 1. The UV–Vis absorption spectra (a) and photoluminescence emission spectra (b) of suspensions of **LPCMP1–4** in THF (10 mg L^{-1}) (for **LPCMP1&2** $\lambda_{\text{ex}} = 380 \text{ nm}$, for **LPCMP3&4** $\lambda_{\text{ex}} = 400 \text{ nm}$). Inset in b) is the photograph of suspensions of the **LPCMP1–4** imaged under irradiation with UV light.

In order to study how the swellability of the material affect its optical properties in more detail, we recorded the photoluminescence emission spectra of suspension of **LPCMP1** in different solvents (**Figure S13**). The swelling of **LPCMP1** in various organic solvents is accompanied by fluorescence changes. Compared with the DMF suspension, an obvious fluorescence enhancement was observed for the suspension in THF and toluene, owing to the expansion of polymer networks and reduced aggregation. The exception was the suspension in methanol, which showed a good swellability, but low fluorescence intensity potentially ascribed the high

polarity of methanol.

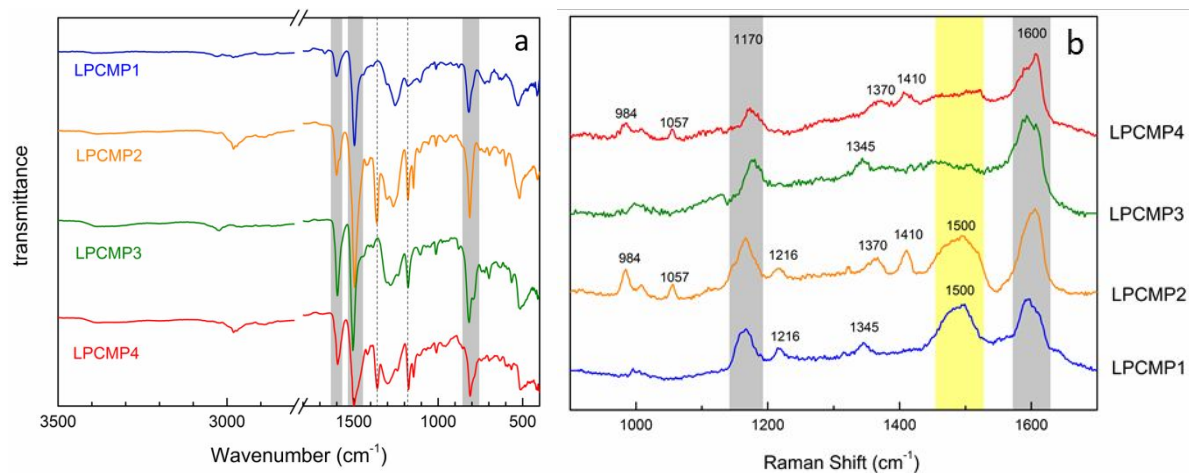


Figure 2. FT-IR (a) and Raman spectra (b) of **LPCMP1–4**

Comparison of the FT-IR spectra of the four polymers (**Figure 2a**) show similarities, such as the peaks at 1600 cm^{-1} , 1500 cm^{-1} , 1180 cm^{-1} and 810 cm^{-1} , which are attributed to the stretching vibrational bands of benzenoid-type secondary amine ($-\text{Ph}-\text{NH}-$), stretching vibrations of the aromatic ring skeleton, stretching vibrational bands of C–N and bending vibrations of $-\text{CH}-$ from substituted benzene, respectively. In contrast to **LPCMP1** and **LPCMP3**, a peak at approximately 1360 cm^{-1} was observed for **LPCMP2** and **LPCMP4**, which is assigned to the characteristic stretching vibrations of the triazine ring. The Raman spectra of all the polymers are shown in **Figure 2b**. All the **LPCMPs** showed two similar peaks at around 1600 cm^{-1} and 1170 cm^{-1} , which are attributed to the C–C stretching of benzene rings and $-\text{CH}-$ in-plane bending from benzenoid rings. For **LPCMP2** and **LPCMP4**, the two weak absorption peaks at 984 cm^{-1} and 1057 cm^{-1} are the characteristic breathing vibrations of the triazine ring. The two weak peaks at 1370 cm^{-1} and 1410 cm^{-1} are assigned to the C–N stretching vibrations of aromatic amines. For **LPCMP1** and **LPCMP2**, a broad peak was observed at 1500 cm^{-1} , assigned to the C–N stretching vibration of the tertiary amine from the tris(4-bromophenyl)amine building block. All these peaks are consistent with the proposed structures of the polymers.

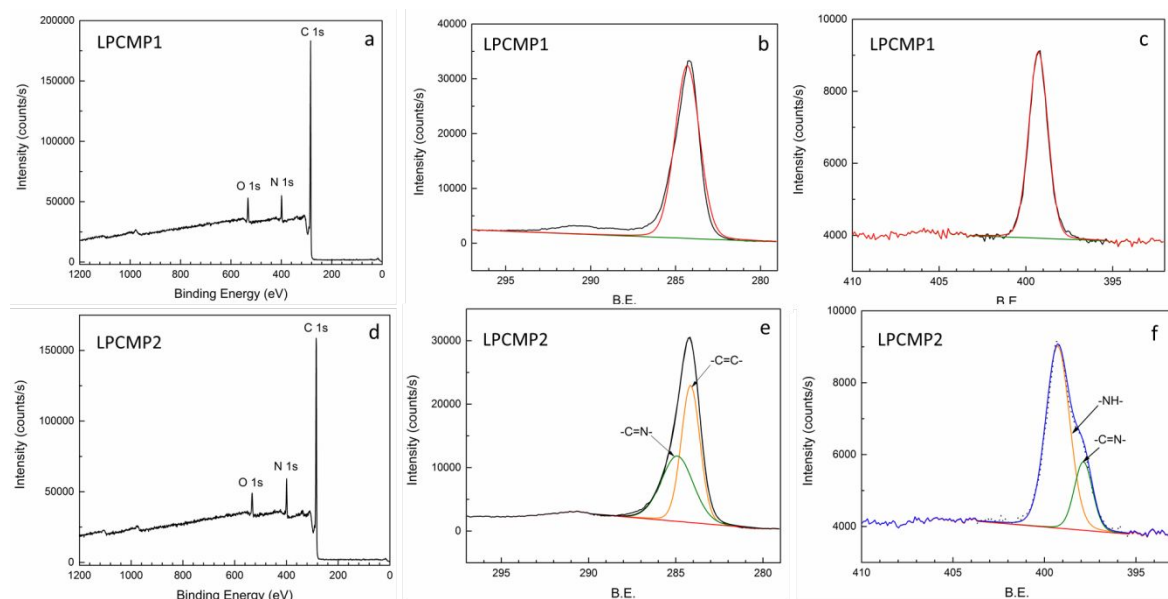


Figure 3. The X-ray photoelectron spectra of **LPCMP1** and **LPCMP2**. (a) and (d) are the survey spectra of **LPCMP1** and **LPCMP2**. (b) and (e) are the high-resolution spectra of C 1s, and (c) and (f) are the high-resolution spectra of N 1s in the two samples, respectively.

In order to further confirm the structures of all the polymers, X-ray photoelectron spectroscopy (XPS) was used to validate the elemental composition and the chemical bond type. As shown in **Figure 3** and **Figure S5**, characteristic carbon and nitrogen peaks were observed in all spectra. The XPS results prove that there was no reaction between the CMP networks and the added inorganic salts, and that all salts were completely removed from the polymers (absence of sodium peaks). The high-resolution XPS spectra of C 1s and N 1s are shown in **Figure 3** and **Figure S5**. For **LPCMP1** and **LPCMP3**, a single peak of the aromatic C centred at 284 eV and a single peak of the amine N centred at 399 eV were observed. For **LPCMP2** and **LPCMP4**, which were constructed from the triazine building block (TPAP), the C 1s and N 1s spectrum could be deconvoluted into two peaks. The weaker peak at 285 eV for the C 1s and at 397 eV for N 1s are the characteristic C and N peaks of the $-C=N-$ moiety from the triazine building block.

Solid-state ^{13}C spectra of **LPCMP1–4** were also acquired (**Figures S6**), which were in good agreement with the proposed structures. Two main resonances at 141 and 128 ppm, which are

assigned to the substituted phenyl carbons and unsubstituted phenyl carbons, respectively, were observed for **LPCMP1–4**. In particular, in the ^{13}C CPMAS NMR spectrum of **LPCMP2** and **LPCMP4**, an additional signal was observed at 171 ppm compared with the ^{13}C CPMAS NMR spectrum of **LPCMP1** and **LPCMP3**, which is attributed to the carbon atoms of the triazine fragment (see the corresponding structures in Scheme 1).

To study the porosity of the materials, sorption analysis using nitrogen as the sorbate molecule was performed. Nitrogen adsorption–desorption isotherms for all the CMPs measured at 77 K are shown in **Figure 4**. A combination of type I and II nitrogen sorption isotherms, according to the IUPAC classification,⁴⁷ were observed for all the polymers. All polymers possess microporous features, which can be inferred from the rapid uptake at a low relative pressure ($P/P_0 = 0-0.1$) shown in the nitrogen adsorption–desorption isotherms. However, the uptake did not reach a plateau, and a continuous increase after adsorption at low relative pressure was observed, which suggests that swelling of the polymer matrices occurred owing to the pressure-dependent dynamic pores structural. In order to confirm this pressure-dependent dynamic structure, two **LPCMP1** samples (80 mg) were washed with methanol and dried in vacuum oven and fume hood, respectively, as shown in **Figure S7**. An obvious volume difference between the two **LPCMP1** samples was observed as further proof of the flexible structure. Upon desorption, a large hysteresis and an open isotherm were observed, caused by the restricted diffusion of the N_2 adsorbate.⁴⁸ The large hysteresis is also indicative of swelling/trapping effects in the flexible polymeric networks, especially for amorphous microporous organic polymers.^{49,50} The BET specific surface area values of **LPCMP1–4** are listed in **Table 2**. **LPCMP1** and **LPCMP3**, synthesized by using 1,3,5-tris(4-aminophenyl)benzene as building block, possess similar BET specific surface area values, much higher than **LPCMP2** and **LPCMP4** that were synthesized with 1,3,5-tris(4-aminophenyl) triazine as building block. One possible reason for the difference in the BET

surface area is that the amino groups in the benzene building blocks are more active than the amino groups in the triazine building blocks when they undergo BH cross coupling and thereby produce polymers with a higher crosslinking degree.⁵¹ The pore size distribution (PSD) profile of the obtained materials is shown in **Figure 4**. **LPCMP2** and **LPCMP4** have similar pore size distributions, both with a dominant pore size (0.72 nm). Compared with **LPCMP2** and **LPCMP4**, a larger dominant pore size located at 1.8 nm were found for **LPCMP1** and **LPCMP3**, which resulted in larger average pore sizes (1.5 and 1.9 nm, respectively). This finding demonstrates that the choice of building block is crucial for the specific surface area and pore size of the CMPs and, more importantly, that the surface area and pore size is tuneable by changing the building blocks.

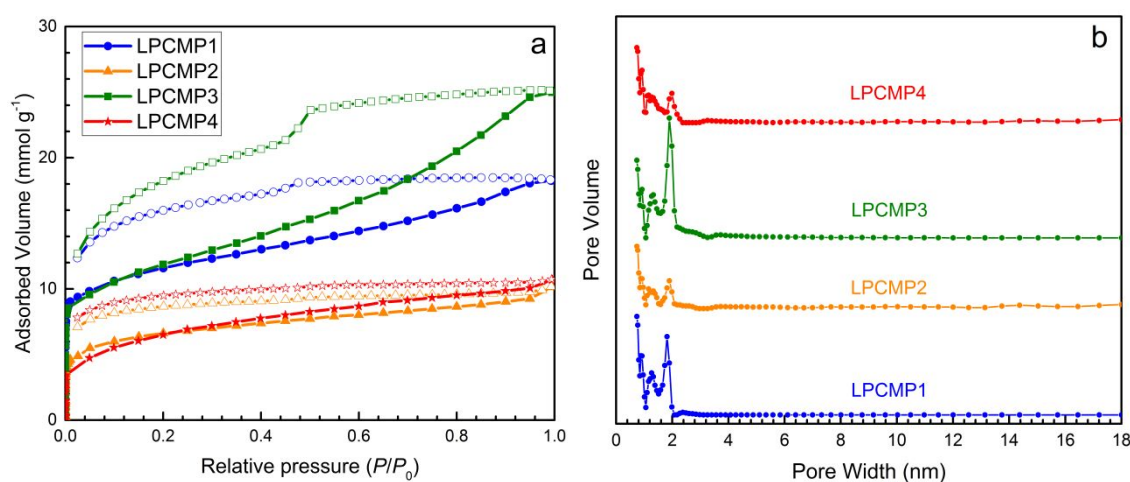


Figure 4. (a) N_2 adsorption–desorption isotherms of **LPCMP1–4** measured at 77 K; the adsorption and desorption branches are marked with solid and open symbols, respectively. (b) The PSD profiles of **LPCMP1–4** calculated by NLDFT.

The CO_2 uptake capacity of all the obtained N-containing **CMPs** was also studied. The CO_2 adsorption isotherms measured at 273 K are shown in **Figure S8**. **LPCMP1** and **LPCMP3**, possessing higher surface areas, exhibit the higher carbon dioxide storage of 3.4 and 3.3 mmol/g (15.0 wt% and 14.5 wt%) at 1.0 bar and 273 K, respectively (see Table 2). The CO_2 adsorption capacities of the two **CMPs** are much higher than the B-H based **CMPs** such as **PTPA-3** (6.5 wt%)²⁰ and **HCMP-1** (7.5 wt%)⁴⁴ and also higher than the other **CMPs** with

similar surface areas, such as FPOP2 (10.2 wt%)¹⁵ and PCZN-8 (14.0 wt%).⁵² For **LPCMP2** and **LPCMP4**, owing to the higher nitrogen content of the triazine building block, the CO₂ uptake capacity still reached 2.5 and 2.2 mmol/g (11.0 wt% and 9.7 wt%), respectively, despite the surface area being less than half of **LPCMP1** and **LPCMP3**.

Table 2. Porosity Properties and CO₂ Uptake Capacities of Polymers

Sample	S _{BET} (m ² g ⁻¹)	V _{total} (cm ³ g ⁻¹) ^a	D _{pore} (nm) ^b	CO ₂ uptake (mmol/g) ^c
LPCMP1	1280	0.59	1.51	3.4
LPCMP2	516	0.30	0.74	2.5
LPCMP3	1340	0.79	1.90	3.3
LPCMP4	570	0.33	0.74	2.2

^a The total pore volume at P/P₀ = 0.99. ^b Data calculated from nitrogen desorption isotherms with the NLDFIT method. ^c Data were obtained at 1.0 bar and 273 K.

LPCMP1 and **LPCMP3** showed surprisingly good swellability after the polymers were washed and dried. **Figure S9** (a) shows **LPCMP1** after the washing and filtration procedure without further drying. **Figure S9**(b) shows **LPCMP1** after drying at 40 °C under vacuum. A significant change in the volume of **LPCMP1** was observed before and after drying: **LPCMP1** shrank 80% after drying. Similar volume changes have only been found in HCPs,⁵³ with such behaviour not reported before for CMPs – an exciting new development for this class of materials.

We carried out a series of experiments to quantify the swellability, Q, of the synthesised CMPs (**Figure 5**).³⁶ The Q values of **LPCMP1-4** in different solvents are listed in **Table 3**. The better swellabilities were obtained for **LPCMP1** and **LPCMP3**, which possess higher BET surface areas and total pore volumes than **LPCMP2** and **LPCMP4**. We believe that the higher crosslinking degree, the richer flexible structure and the more dynamic pores of **LPCMP1** and **LPCMP3** enable an increase in the swelling of the network. The greatest degree of swelling was obtained for the **LPCMP1** and **LPCMP3** with methanol (Q= 16.5 and 16.3 mL g⁻¹ respectively) and the least swelling obtained when DMF was used as the solvent (Q= 8.1 and

9.1 mL g⁻¹ respectively). Notably, the Q values observed are even higher than the swelling of HCPs derived from in fluorobenzene and toluene (with Q values of 15.7 mL g⁻¹ in DMF).⁵³ These results demonstrate that the novel CMPs possess unparalleled and uniquely flexible networks, fully consistent with the nitrogen sorption isotherms.

The swellability of **LPCMP1-NS** was also studied, as shown in **Figure S10**. Compared with **LPCMP1**, the swelling values of **LPCMP1-NS** are negligible, indicating that the BXJ approach and addition of salt plays an essential role in improving the swelling performance.

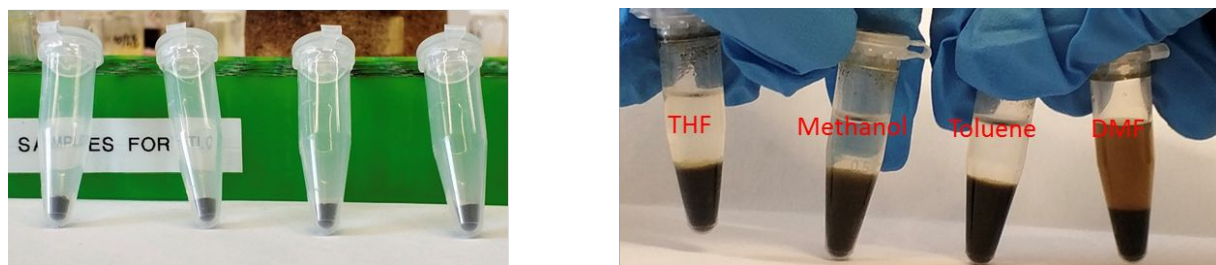


Figure 5. Images of **LPCMP1** before and after swelling with THF, methanol, toluene and DMF, respectively.

Table 3. Swellability (Q) for **LPCMP1-4** against THF, methanol, toluene and DMF.

Sample	Swellability Q (mL g ⁻¹)			
	THF	Methanol	Toluene	DMF
LPCMP1	13.3	16.5	16.0	8.1
LPCMP2	14.5	11.3	11.2	9.8
LPCMP3	16.2	16.2	13.3	9.1
LPCMP4	13.5	11.4	11.7	8.8

Vapor adsorption

The CMPs with high porosity and excellent swellability potentially allow access to the pores for a variety of small vapor molecules. We therefore explored the ability of our CMPs to take up toluene and methanol vapors, as these two volatile organic compounds (VOC) are major air pollutants in the indoor atmosphere.⁵⁴ Methanol is the simplest of the alcohols, and is used, for

example, as a solvent, an alternative fuel, and as feedstock for producing other chemicals.⁵⁵ It is the second most abundant VOC in the atmosphere after methane and promotes the formation of photochemical smog and is also harmful to the nervous system of humans.⁵⁶ Toluene is also a typical VOC pollutant and has been utilized in many chemical manufacturing processes, including as solvent in paints, inks, and in the adhesives industries.⁵⁷ Toluene affects the human nervous system directly, and may lead to acute headaches, dizziness, or unconsciousness.⁵⁸ There is thus a clear need to explore effective adsorbents for VOC such as methanol and toluene.

Toluene adsorption isotherms of the four obtained polymers at 298 K are shown in **Figure 6**. For **LPCMP2** and **LPCMP4**, Type-I isotherms⁴⁷ were observed, indicative of monolayer adsorption (i.e., at low pressure, because of the strong interaction between the solid surface of the adsorbent and the vapour adsorbate, the amount adsorbed increases with a rise in pressure). However, after the first adsorbed layer reached saturation, there was no obvious change in the amount of adsorption upon further increasing pressure, indicating the lack of multilayer adsorption. For the **LPCMP1** and **LPCMP3**, Type-IV isotherms⁴⁷ were observed. Different from the isotherms of **LPCMP2** and **LPCMP4**, after rapid uptake at a low relative pressure, the adsorption continued to gradually increase with increasing pressure, indicative of multilayer adsorption after saturation of the first adsorbed layer. This behaviour can be explained by the bigger pore size and better swellability of **LPCMP1** and **LPCMP3**. In addition, there is an obvious desorption hysteresis for all four polymers, which is indicative of weak host–guest interactions (π - π stacking), and capillary condensation.⁴⁷ Owing to the higher specific surface area and better swellability, both **LPCMP1** and **LPCMP3** show excellent vapour adsorption capacity for toluene. The uptake capacities reached 116 wt% and 114 wt%, respectively, at the saturated vapor pressure. The values are comparable with the highest reported toluene adsorption capacity porous materials, such as **CPOP-15** (147 wt%),⁵⁹ **FPOP-1** (98 wt%)¹⁵ and even **PAF-1** (136 wt%) with an ultrahigh specific surface area.⁶⁰

The methanol adsorption isotherms of the four obtained polymers at 298 K are shown in **Figure 6**. Interestingly, unlike the isotherms for toluene, all four the methanol isotherms are Type-III isotherms, which indicate unrestricted multilayer formation. This behaviour occurs because lateral interactions between adsorbed methanol molecules (hydrogen-bonding interaction) are stronger in comparison to interactions between the adsorbent surface and adsorbate (no π - π stacking interactions).⁴⁷ Furthermore, negligible hysteresis was detected for all polymers, which, in general, points to a lower required regeneration energy needed for subsequent reuse. The maximum methanol uptake capacities of **LPCMP1** and **LPCMP3** are remarkably high; notably, 250 wt% and 215 wt% for **LPCMP1** and **LPCMP3**, respectively, at methanol saturated vapor pressure. To our knowledge, this adsorption value is the highest recorded when compared with other CMPs, HCPs, MOFs and porous carbons (as shown in Table S2). The previous record for methanol adsorption capacity at 115 wt% was held by **MIL-101(Cr)**, a MOF material for which the BET surface area is significantly higher at 4230 m² g⁻¹. **LPCMP1** and **LPCMP3** show approximately twice the methanol adsorption capacity, despite their surface areas being only approximately one quarter of that determined for **MIL-101(Cr)**. The outstanding uptake capacity for organic vapors coupled to superior swellability provide very promising application opportunities for these polymers in the area of hazardous organic vapor elimination (including toxic chemical warfare agent uptake and removal).

Three cycles of adsorption–desorption tests of **LPCMP1** have been carried out to further study the repeatability and reusability of **LPCMP1** for the uptake of toluene and methanol vapours. At the end of each isotherm, **LPCMP1** was kept at 150 °C under vacuum for 3 h to ensure full vapour desorption. As shown in **Figure S11**, virtually no change of the uptake capacity for toluene or methanol was observed after three cycles. **LPCMP1** shows good stability and repeatability for organic vapour uptake, which is crucial for its practical application.

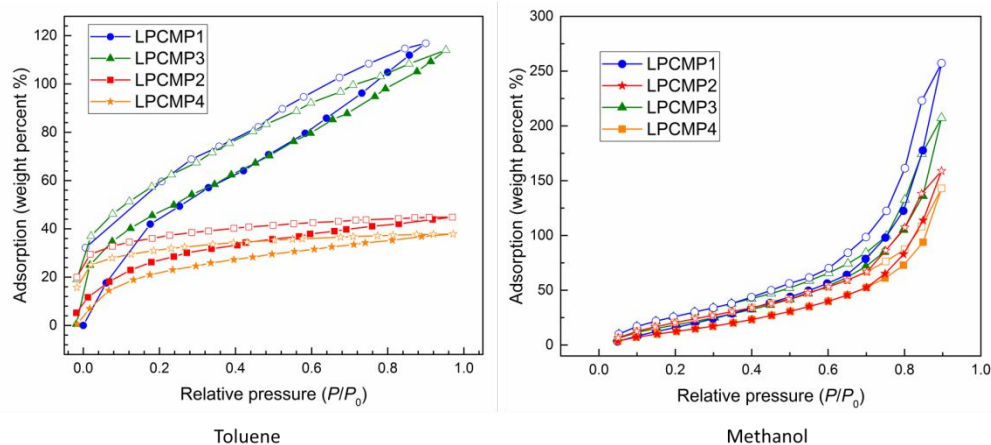


Figure 6. Toluene and methanol adsorption isotherms of **LPCMP1–4** at 298 K (the adsorption and desorption branches are labelled with solid and open symbols, respectively)

Chemical sensing experiments were conducted by adding different concentrations of nitroaromatics (TNT, NP, DNB, DNT, NB) into suspensions of **LPCMP1–4** (10 mg L^{-1} in THF) and monitoring the luminescence quenching. As shown in **Figure 7**, for all the CMPs, the intensity of the fluorescence emission gradually decreased upon increasing the concentration of TNT. Similar fluorescence quenching was observed when NP, DNB, DNT and NB were investigated, but the quenching was less efficient than for TNT. This fluorescence quenching phenomenon can be explained by a donor–acceptor electron-transfer mechanism. When nitroaromatics are added to the CMP suspensions π -stacking interactions occur between the conjugated networks of the CMPs and the nitroaromatics. Upon excitation, electrons are transferred from the CMPs’ conduction band to the lowest unoccupied molecular orbital (LUMO) of the nitroaromatics, which results in the observed quenching.²²

In order to quantify the quenching efficiencies of the different CMPs for different nitroaromatics, the Stern–Volmer equation ($I_0 / I = K_{SV} [C]$, with I_0 the initial fluorescence intensity, I the fluorescence intensity measured at different concentration of nitroaromatics and K_{SV} the Stern–Volmer constant) was applied. The Stern–Volmer plots for all CMPs are shown in **Figure 8**. The Stern–Volmer plots show a linear relationship between the I_0 / I and the

concentration of nitroaromatics. Moreover, the quenching efficiencies can be quantified by the slope (K_{sv}) of the lines. As shown in **Table 4**, for all the CMPs, TNT gives the highest quenching efficiencies (highest K_{sv} value), with descending quenching efficiency in the following order: TNT>NP> DB> DT> NB. The LUMO levels of all the nitroaromatics were also calculated using density functional theory (DFT) calculations which were performed with the GaussView 5.0 and MobaXterm software using the B3LYP functional and the 6-31G(d) basis set. The LUMO energy level order from low to high is TNT< NP< DB< DT< NB, which matches the quenching efficiency exactly. This trend indicates that excited electrons from the CMP networks can be transferred to the LUMO of TNT with highest efficiency, with the obtained results in accordance with the quenching efficiency order. The detection limits, which were calculated as three times the standard deviation of the background noise from the calibration curves, for the determination of TNT for **LPCMP1** and **LPCMP2** were 5.85×10^{-6} mol L⁻¹ and 3.64×10^{-6} mol L⁻¹, respectively. It should be mentioned that the Stern–Volmer constants (K_{sv}) of **LPCMP2** and **LPCMP3** for TNT (4147 and 1245 M⁻¹, respectively), which are comparable to other reported CMPs chemosensors,⁶¹ are significantly higher than for the other nitroaromatics (see Table 4). This result indicates that both **LPCMP2** and **LPCMP4** exhibit high selectivity for TNT and may be suitable as new candidates to selectively detect TNT for security or environmental applications.

Table 4. K_{sv} value of **LPCMP1-4** for the different nitroaromatics

Material	K_{sv} (M ⁻¹)				
	TNT	NP	DB	DT	NB
LPCMP1	2563	602	283	245	89
LPCMP2	4147	179	138	65	32
LPCMP3	886	286	163	111	20
LPCMP4	1245	88	61	40	11

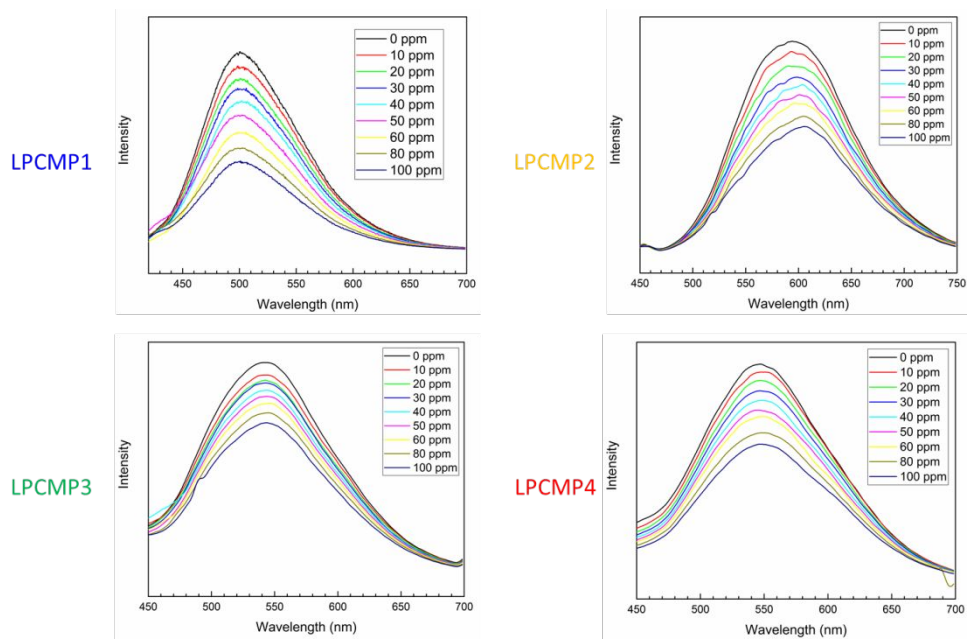


Figure 7. Photoluminescence quenching of LPCMP1-4 with various concentrations of TNT (for **LPCMP1**, **2** $\lambda_{\text{ex}} = 380$ nm for **LPCMP3**, **4** $\lambda_{\text{ex}} = 400$ nm)

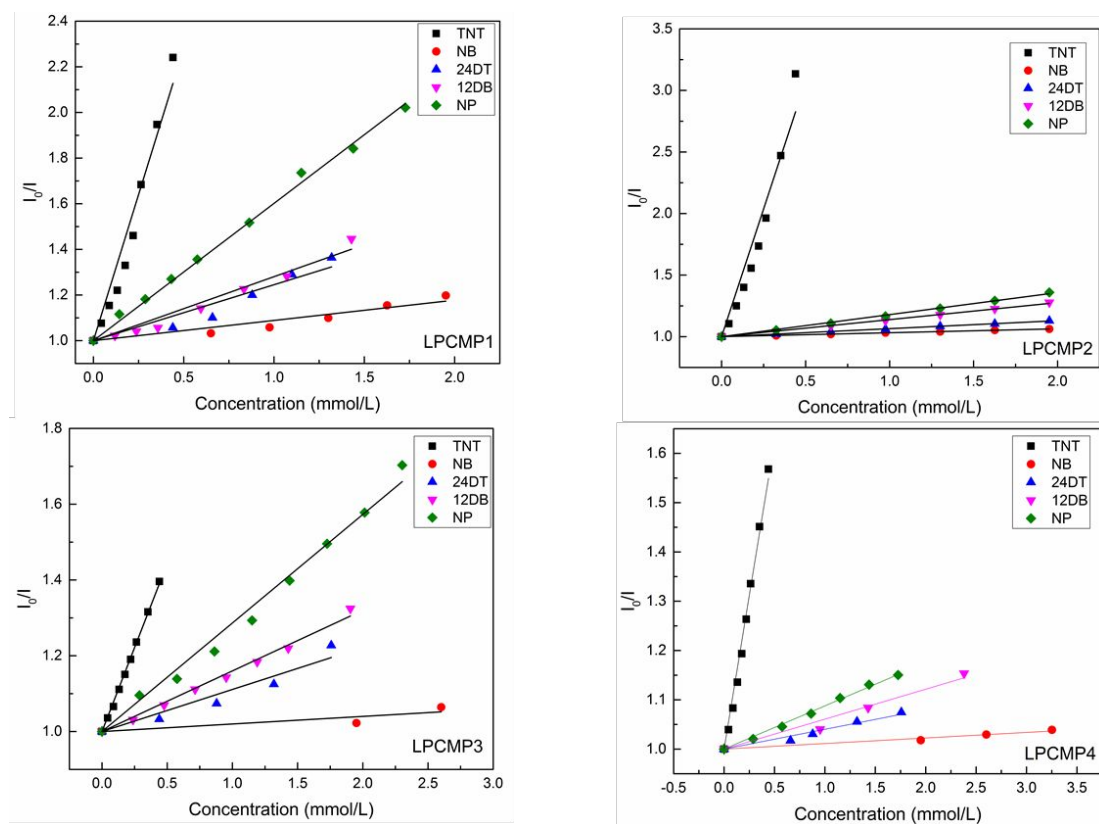


Figure 8. Stern–Volmer plots of **LPCMP1-4**

Conclusion

In conclusion, four new conjugated microporous polymers were synthesised by BH cross coupling reaction. The surface areas and pore size distributions of the polymers were tuned by changing the chemical structure of the building blocks, varying the ratios of bromine and amine building blocks and application of our recently developed BXJ method. The produced CMP materials possess high Brunauer–Emmett–Teller (BET) specific surface areas, high chemical and thermal stabilities and are exhibit luminescent. They show very sensitive and selective fluorescence quenching in the presence of trace amount of nitroaromatic compounds. In terms of environmental and security concerns, the present study suggests that these materials may be used as fluorescent sensors for nitroaromatics. Moreover, all the CMPs show outstanding ability to take up large volumes of organic liquids (including toluene, tetrahydrofuran (THF) and methanol) by swelling of the porous networks. This unique and little-studied property has the potential to be utilised in environmental and related applications. Owing to their excellent swellability, we further studied the adsorption capacity of the CMPs for different toxic volatile organic vapours, specifically toluene and methanol. Impressively, **LPCMP1** and **LPCM3** exhibit excellent toluene adsorption capacity, while they possess the highest methanol adsorption capacity by a factor of two when compared with the best published data. These materials show great potential for application in indoor air quality remediation, general hazardous organic vapour elimination and chemical warfare agent uptake – wide application of our materials is envisaged.

Acknowledgements

L.P. acknowledges a Newton Fellowship from the Royal Society for funding (Grant Reference: NF170361). Z.L.L acknowledges China Scholarship Council (CSC). BET data were collected on a Quantachrome Autosorb iQ bought under EPSRC CDT Capital grant (EP/K035746/1).

Supporting Information

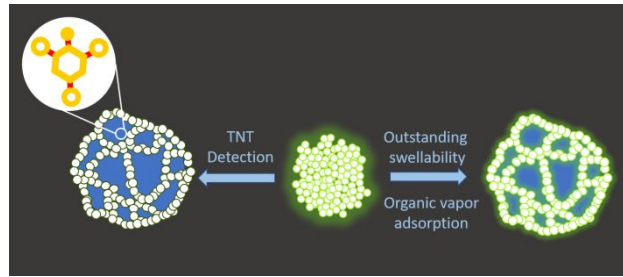
Synthesis of TAPT and TBPE, thermogravimetric analysis of LPCMP1-4, SEM images of LPCMP1-4, X-ray photoelectron spectra of LPCMP3 and LPCMP4, Solid-state ¹³C CPMAS NMR spectra of LPCMP1-4, images of LPCMP1 dried under atmospheric pressure and vacuum oven, CO₂ adsorption isotherms for LPCMP1-4 at 273 K, LPCMP1-NS and LPCMP1 before and after dispersing in methanol, uptake capacity of LPCMP1 for toluene and methanol after three cycles, methanol adsorption properties for LPCMP1 and LPCMP3 in comparison with other high-performing porous materials, The photographs of suspensions of the LPCMP1 in pure THF and TNT solution under irradiation with UV light, photoluminescence emission spectra of suspension of LPCMP1 with different organic solvents and summarization of the cores and linkers of the B-H based CMPs.

References

1. Wu, D.; Xu, F.; Sun, B.; Fu, R.; He, H.; Matyjaszewski, K., Design and Preparation of Porous Polymers. *Chem. Rev.* **2012**, *112* (7), 3959-4015.
2. Cooper, A. I., Conjugated Microporous Polymers. *Adv. Mater.*, **2009**, *21* (12), 1291-1295.
3. Xu, Y.; Jin, S.; Xu, H.; Nagai, A.; Jiang, D., Conjugated Microporous Polymers: Design, Synthesis and Application. *Chem. Soc. Rev.*, **2013**, *42* (20), 8012-8031.
4. Feng, X.; Ding, X.; Jiang, D., Covalent organic frameworks. *Chem. Soc. Rev.*, **2012**, *41* (18), 6010-6022.
5. El-Kaderi, H. M.; Hunt, J. R.; Mendoza-Cortes, J. L.; Cote, A. P.; Taylor, R. E.; O'Keeffe, M.; Yaghi, O. M., Designed Synthesis of 3D Covalent Organic Frameworks. *Science*, **2007**, *316* (5822), 268-272.
6. McKeown, N. B.; Budd, P. M., Polymers of Intrinsic Microporosity (PIMs): Organic Materials for Membrane Separations, Heterogeneous Catalysis and Hydrogen Storage. *Chem. Soc. Rev.*, **2006**, *35* (8), 675-683.
7. McKeown, N. B.; Budd, P. M., Exploitation of Intrinsic Microporosity in Polymer-Based Materials. *Macromolecules*, **2010**, *43* (12), 5163-5176.
8. Ben, T.; Pei, C.; Zhang, D.; Xu, J.; Deng, F.; Jing, X.; Qiu, S., Gas Storage in Porous Aromatic Frameworks (PAFs). *Energy Environ. Sci.*, **2011**, *4* (10), 3991-3999.
9. Xu, S.; Luo, Y.; Tan, B., Recent Development of Hypercrosslinked Microporous Organic Polymers. *Macromol. Rapid. Comm.*, **2013**, *34* (6), 471-484.
10. Weber, J.; Thomas, A., Toward Stable Interfaces in Conjugated Polymers: Microporous Poly(P-Phenylene) and Poly(Phenyleneethynylene) Based on a Spirobifluorene Building Block. *J. Am. Chem. Soc.*, **2008**, *130* (20), 6334-6335.
11. Jiang, J.-X.; Su, F.; Trewin, A.; Wood, C. D.; Campbell, N. L.; Niu, H.; Dickinson, C.; Ganin, A. Y.; Rosseinsky, M. J.; Khimyak, Y. Z.; Cooper, A. I., Conjugated Microporous Poly(aryleneethynylene) Networks. *Angew. Chem. Int. Edit.*, **2007**, *46* (45), 8574-8578.
12. Schmidt, J.; Werner, M.; Thomas, A., Conjugated Microporous Polymer Networks via Yamamoto Polymerization. *Macromolecules*, **2009**, *42* (13), 4426-4429.
13. Yuan, S.; Dorney, B.; White, D.; Kirklin, S.; Zapol, P.; Yu, L.; Liu, D.-J., Microporous Polyphenylenes with Tunable Pore Size for Hydrogen Storage. *Chem. Comm.*, **2010**, *46* (25), 4547-4549.
14. Li, L.; Ren, H.; Yuan, Y.; Yu, G.; Zhu, G., Construction and Adsorption Properties of Porous Aromatic Frameworks via AlCl₃-Triggered Coupling Polymerization. *J. Mater. Chem. A*, **2014**, *2* (29), 11091-11098.
15. Liu, D.-P.; Chen, Q.; Zhao, Y.-C.; Zhang, L.-M.; Qi, A.-D.; Han, B.-H., Fluorinated Porous Organic Polymers via Direct C-H Arylation Polycondensation. *ACS Macro Letters*, **2013**, *2* (6), 522-526.
16. Bohra, H.; Li, P.; Yang, C.; Zhao, Y.; Wang, M., "Greener" and Modular Synthesis of Triazine-Based Conjugated Porous Polymers via Direct Arylation Polymerization: Structure-function Relationship and Photocatalytic Application. *Polym. Chem.* **2018**, *9* (15), 1972-1982.
17. Chen, Q.; Luo, M.; Hammershoj, P.; Zhou, D.; Han, Y.; Laursen, B. W.; Yan, C.-G.; Han, B.-H., Microporous Polycarbazole with High Specific Surface Area for Gas Storage and Separation. *J. Am. Chem. Soc.*, **2012**, *134* (14), 6084-6087.
18. Zhang, C.; He, Y.; Mu, P.; Wang, X.; He, Q.; Chen, Y.; Zeng, J.; Wang, F.; Xu, Y.; Jiang, J.-X., Toward High Performance Thiophene-Containing Conjugated Microporous Polymer Anodes for Lithium-Ion Batteries through Structure Design. *Adv. Funct. Mater.*, **2018**, *28* (4), 1705432.
19. Jiang, J. X.; Su, F.; Niu, H.; Wood, C. D.; Campbell, N. L.; Khimyak, Y. Z.; Cooper, A. I., Conjugated Microporous Poly(phenylene butadiynylene)s. *Chem. Commun.*, **2008**, *4*, 486-488.
20. Liao, Y.; Weber, J.; Faul, C. F. J., Conjugated Microporous Polytriphenylamine Networks. *Chem. Commun.*, **2014**, *50* (59), 8002-8005.
21. Liao, Y.; Wang, H.; Zhu, M.; Thomas, A., Efficient Supercapacitor Energy Storage Using Conjugated Microporous Polymer Networks Synthesized from Buchwald-Hartwig Coupling. *Adv. Mater.*, **2018**, *30* (12), 1705710.

-
22. Liu, X. M.; Xu, Y. H.; Jiang, D. L., Conjugated Microporous Polymers as Molecular Sensing Devices: Microporous Architecture Enables Rapid Response and Enhances Sensitivity in Fluorescence-On and Fluorescence-Off Sensing. *J. Am. Chem. Soc.*, **2012**, *134* (21), 8738-8741.
23. Pan, L.; Xu, M.-Y.; Feng, L.-J.; Chen, Q.; He, Y.-J.; Han, B.-H., Conjugated Microporous Polycarbazole Containing Tris(2-Phenylpyridine)Iridium(III) Complexes: Phosphorescence, Porosity, and Heterogeneous Organic Photocatalysis. *Poly. Chem.*, **2016**, *7* (12), 2299-2307.
24. Chen, J.; Yan, W.; Townsend, E. J.; Feng, J.; Pan, L.; Del Angel Hernandez, V.; Faul, C. F. J., Tuneable Surface Area, Porosity and Function in Conjugated Microporous Polymers. *Angew. Chem. Int. Edit.*, **2019**, *58* (34), 11715-11719.
25. Wang, H.; Cheng, Z.; Liao, Y.; Li, J.; Weber, J.; Thomas, A.; Faul, C. F. J., Conjugated Microporous Polycarbazole Networks as Precursors for Nitrogen-Enriched Microporous Carbons for CO₂ Storage and Electrochemical Capacitors. *Chem. Mater.*, **2017**, *29* (11), 4885-4893.
26. Wang, S.; Liu, Y.; Yu, Y.; Du, J.; Cui, Y.; Song, X.; Liang, Z., Conjugated Microporous Polymers Based on Biphenylene for CO₂ Adsorption and Luminescence Detection of Nitroaromatic Compounds. *New J. Chem.*, **2018**, *42* (12), 9482-9487.
27. Gu, C.; Huang, N.; Gao, J.; Xu, F.; Xu, Y.; Jiang, D., Controlled Synthesis of Conjugated Microporous Polymer Films: Versatile Platforms for Highly Sensitive and Label-Free Chemo- and Biosensing. *Angew. Chem. Int. Edit.*, **2014**, *53* (19), 4850-4855.
28. Tsyurupa, M. P.; Davankov, V. A., Hypercrosslinked Polymers: Basic Principle of Preparing the New Class of Polymeric Materials. *React. Funct. Poly.*, **2002**, *53* (2-3), 193-203.
29. Davankov, V. A.; Tsyurupa, M. P., Structure and Properties of Hypercrosslinked Polystyrene - the 1st Representative of a New Class of Polymer Networks. *React. Poly.*, **1990**, *13* (1-2), 27-42.
30. Tang, X. S.; Jia, W.; Yan, J., Water-swelling Hydrophobic Porous Copolymer Resins Based on Divinylbenzene and Acrylonitrile. I. Water-swelling Behavior. *J. Appl. Polym. Sci.*, **2004**, *94* (5), 2041-2049.
31. Detoni, C.; Gierlich, C. H.; Rose, M.; Palkovits, R., Selective Liquid Phase Adsorption of 5-Hydroxymethylfurfural on Nanoporous Hyper-Cross-Linked Polymers. *ACS Sustainable Chemistry & Engineering* **2014**, *2* (10), 2407-2415.
32. Podlesnyuk, V. V.; Hradil, J.; Kralova, E., Sorption of Organic Vapours by Macroporous and Hypercrosslinked Polymeric Adsorbents. *React. Funct. Poly.*, **1999**, *42* (3), 181-191.
33. Kiseleva, M. G.; Radchenko, L. V.; Nesterenko, P. N., Ion-exchange Properties of Hypercrosslinked Polystyrene Impregnated with Methyl Orange. *J. Chromatogr. A*, **2001**, *920* (1-2), 79-85.
34. Penner, N. A.; Nesterenko, P. N., Application of Neutral Hydrophobic Hypercrosslinked Polystyrene to the Separation of Inorganic Anions by Ion Chromatography. *J. Chromatogr. A*, **2000**, *884* (1-2), 41-51.
35. Fontanals, N.; Galia, M.; Cormack, P. A. G.; Marce, R. M.; Sherrington, D. C.; Borrull, F., Evaluation of a New Hypercrosslinked Polymer as a Sorbent for Solid-Phase Extraction of Polar Compounds. *J. Chromatogr. A*, **2005**, *1075* (1-2), 51-56.
36. Pan, B. C.; Xiong, Y.; Su, Q.; Li, A. M.; Chen, J. L.; Zhang, Q. X., Role of Amination of a Polymeric Adsorbent on Phenol Adsorption from Aqueous Solution. *Chemosphere*, **2003**, *51* (9), 953-962.
37. Banerjee, D.; Hu, Z.; Li, J., Luminescent Metal-Organic Frameworks as Explosive Sensors. *Dalton T.*, **2014**, *43* (28), 10668-10685.
38. Sun, X. C.; Wang, Y.; Lei, Y., Fluorescence Based Explosive Detection: from Mechanisms to Sensory Materials. *Chem. Soc. Rev.*, **2015**, *44* (22), 8019-8061.
39. Abadin, H.; Smith, C.; Ingerman, L.; Ingerman, L.; Lladós, F.; Barber, L.; Plewak D.; Diamond, L., Toxicological Profile for RDX. Atlanta (GA): Agency for Toxic Substances and Disease Registry (US); 2012 Jan. 3, HEALTH EFFECTS. Available from: <https://www.ncbi.nlm.nih.gov/books/NBK154146/>.
40. J. Akhavan, Chemistry of Explosives, *Royal Society of Chemistry*, Cambridge, 2004.
41. Chen, D.; Liu, C.; Tang, J.; Luo, L.; Yu, G., Fluorescent Porous Organic Polymers. *Polym. Chem.* **2019**, *10* (10), 1168-1181.

-
42. Geng, T.; Zhu, Z.; Wang, X.; Xia, H.; Wang, Y.; Li, D., Poly{tris[4-(2-Thienyl)phenyl]amine} Fluorescent Conjugated Microporous Polymer for Selectively Sensing Picric Acid. *Sensors and Actuators B: Chemical* **2017**, *244*, 334-343.
43. Chen, Q.; Wang, J.-X.; Yang, F.; Zhou, D.; Bian, N.; Zhang, X.-J.; Yan, C.-G.; Han, B.-H., Tetraphenylethylene-based Fluorescent Porous Organic Polymers: Preparation, Gas Sorption Properties and Photoluminescence Properties. *J. Mater. Chem.*, **2011**, *21* (35), 13554-13560.
44. Liao, Y.; Weber, J.; Mills, B. M.; Ren, Z.; Faul, C. F. J., Highly Efficient and Reversible Iodine Capture in Hexaphenylbenzene-Based Conjugated Microporous Polymers. *Macromolecules* **2016**, *49* (17), 6322-6333.
45. Chen, D.; Liu, C.; Tang, J.; Luo, L.; Yu, G., Fluorescent Porous Organic Polymers. *Polym. Chem.*, **2019**, *10* (10), 1168-1181.
46. Bonillo, B.; Sprick, R. S.; Cooper, A. I., Tuning Photophysical Properties in Conjugated Microporous Polymers by Comonomer Doping Strategies. *Chem. Mater.*, **2016**, *28* (10), 3469-3480.
47. Reporting Physisorption Data for Gas/Solid Systems. In *Handbook of Heterogeneous Catalysis*, 1217-1230.
48. Jeromenok, J.; Weber, J., Restricted Access: on the Nature of Adsorption/Desorption Hysteresis in Amorphous, Microporous Polymeric Materials. *Langmuir*, **2013**, *29* (42), 12982-12989.
49. Rose, M.; Boehlmann, W.; Sabo, M.; Kaskel, S., Element-Organic Frameworks with High Permanent Porosity. *Chem. Comm.*, **2008**, (21), 2462-2464.
50. Weber, J.; Antonietti, M.; Thomas, A., Microporous Networks of High-Performance Polymers: Elastic Deformations and Gas Sorption Properties. *Macromolecules* **2008**, *41* (8), 2880-2885.
51. Ruiz-Castillo, P.; Buchwald, S. L., Applications of Palladium-Catalyzed C-N Cross-Coupling Reactions. *Chem. Rev.*, **2016**, *116* (19), 12564-12649.
52. Liao, Y.; Cheng, Z.; Trunk, M.; Thomas, A., Targeted Control Over the Porosities and Functionalities of Conjugated Microporous Polycarbazole Networks for CO₂-Selective Capture and H₂ Storage. *Polym. Chem.*, **2017**, *8* (46), 7240-7247.
53. Wilson, C.; Main, M. J.; Cooper, N. J.; Briggs, M. E.; Cooper, A. I.; Adams, D. J., Swellable Functional Hypercrosslinked Polymer Networks for the Uptake of Chemical Warfare Agents. *Polym. Chem.*, **2017**, *8* (12), 1914-1922.
54. Qin, W.; Cao, W.; Liu, H.; Li, Z.; Li, Y., Metal-organic Framework MIL-101 Doped with Palladium for Toluene Adsorption and Hydrogen Storage. *RSC Adv.*, **2014**, *4* (5), 2414-2420.
55. Ma, X.; Li, L.; Zeng, Z.; Chen, R.; Wang, C.; Zhou, K.; Su, C.; Li, H., Synthesis of Nitrogen-Rich Nanoporous Carbon Materials With C₃N-Type From ZIF-8 For Methanol Adsorption. *Chem. Eng. J.*, **2019**, *363*, 49-56.
56. Schröder, E., Methanol Adsorption on Graphene. *J. Nanomater.*, **2013**, *2013*, 1-6.
57. Vellingiri, K.; Kumar, P.; Deep, A.; Kim, K.-H., Metal-organic Frameworks for the Adsorption of Gaseous Toluene Under Ambient Temperature and Pressure. *Chem. Eng. J.*, **2017**, *307*, 1116-1126.
58. Hudak, A.; Ungvary, G., Embryotoxic Effects of Benzene and Its Methyl Derivatives: Toluene, Xylene. *Toxicology*, **1978**, *11* (1), 55-63.
59. Zhu, J.-H.; Chen, Q.; Sui, Z.-Y.; Pan, L.; Yu, J.; Han, B.-H., Preparation and Adsorption Performance of Cross-Linked Porous Polycarbazoles. *J. Mater. Chem. A*, **2014**, *2* (38), 16181-16189.
60. Ben, T.; Ren, H.; Ma, S.; Cao, D.; Lan, J.; Jing, X.; Wang, W.; Xu, J.; Deng, F.; Simmons, J. M.; Qiu, S.; Zhu, G., Targeted Synthesis of a Porous Aromatic Framework with High Stability and Exceptionally High Surface Area. *Angew. Chem. Int. Edit.*, **2009**, *48* (50), 9457-9460.
61. Xiang, Z.; Cao, D., Synthesis of Luminescent Covalent-Organic Polymers For Detecting Nitroaromatic Explosives and Small Organic Molecules. *Macromol. Rapid. Comm.*, **2012**, *33* (14), 1184-1190.



For Table of Contents Only